JCTC Journal of Chemical Theory and Computation

Conformational Studies of Methyl β-D-Arabinofuranoside Using the AMBER/GLYCAM Approach

Hashem A. Taha,[†] Norberto Castillo,[†] Pierre-Nicholas Roy,*[,‡] and Todd L. Lowary*[,†]

Department of Chemistry and Alberta Ingenuity Centre for Carbohydrate Science, Gunning-Lemieux Chemistry Centre, University of Alberta, Edmonton, Alberta, Canada T6G 2G2, and Department of Chemistry, University of Waterloo, Waterloo, Ontario, Canada N2L 3G1

Received September 12, 2008

Abstract: Furanosides are important constituents of a number of glycoconjugates from many microorganisms. The highly flexible nature of these furanosyl moieties is believed to contribute significantly to their role in biological processes. Therefore, an understanding of the conformational preferences of these molecules is an important area of research. As part of a larger program involved in the conformational analysis of mycobacterial oligofuranosides, molecular dynamics simulations on methyl β-D-arabinofuranoside (**3**) have been carried out using the AMBER forcefield and the GLYCAM carbohydrate parameter set. This approach was used to predict the rotamer population distribution about the hydroxymethyl group (C4−C5 bond) as well as the ring puckering of this flexible ring system. Comparison of the conformer distributions obtained during the simulation of **3** using the TIP3P water model with those obtained by analysis of $^{1}H-^{1}H$ coupling constant data indicated that this water model was insufficient to describe the solvation of this system. However, the use of the TIP4P and TIP5P models led to improved agreement with conformer populations obtained from NMR data.

Introduction

Tuberculosis (TB) is a significant world health concern that affects one-third of the world's population and kills nearly three million people annually.[1] The dramatic increase in drug-resistant strains of the bacterium that causes TB, *Mycobacterium tuberculosis,* has heightened interest in the development of novel vaccines and antibiotics for the prevention and treatment of the disease.[2−4] The treatment of bacterial disease often involves the use of antibiotics that act by inhibiting the biosynthesis of the bacterial cell wall.[5−7] Some of the clinically used anti-TB drugs act in this fashion,[8] and the mycobacterial cell wall has attracted significant attention in the development of new drugs for the treatment of this disease.[2,9,10]

The cell wall in mycobacteria, a complex array of polysaccharides, proteins, lipids, and glycolipids,[11] consists of two major carbohydrate components, an arabinogalactan (AG) and a lipoarabinomannan (LAM). These polymers contain arabinose and galactose residues present exclusively in the furanose ring form. Compared to their pyranose counterparts, these five-membered rings are the least thermodynamically stable forms of most monosaccharides. Although pyranosides generally exist in well-defined energetically favorable chair conformations that have little ring strain, furanosides have increased ring strain. Consequently, furanoside rings are flexible species that can adopt several conformational states, typically separated by low energy barriers.[12] The inherent flexibility of these five-membered ring carbohydrates is postulated[13] to play a role in the protection of the organism against its environment by providing a malleable scaffold that promotes the ideal packing of the mycolic acid residues attached to the terminal ends of the AG.[11] These densely packed lipids form a lipophilic barrier at the outer part of the cell wall that protects the organism against both the passage of antibiotics and the immune system of the infected host.[14]

* Corresponding author e-mail: pnroy@uwtaerloo.ca (P.-N.R.), todd.lowary@ualberta.ca (T.L.L.).

[†] University of Alberta.

[‡] University of Waterloo.

10.1021/ct800384h CCC: $40.75
Published on Web 01/08/2009

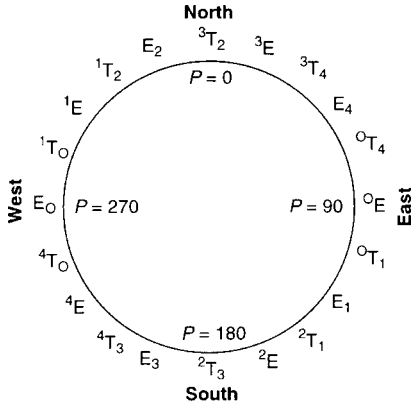

Figure 1. Pseudorotational itinerary for a D-aldofuranose ring.

The critical role that the arabinofuranose ring system plays in the cell wall structure of mycobacteria has prompted our interest in understanding the conformational preferences of oligosaccharides containing arabinofuranose rings.[12,15−19] This work has been driven by hope that this knowledge will aid in the design of potential inhibitors of the enzymes involved in biosynthesis of the arabinofuranose-containing portions of the mycobacterial cell wall.[9]

The conformational preferences of furanose rings are difficult to determine due to their great flexibility; these rings can adopt various envelope and twist conformations as depicted on the pseudorotational itinerary[20] (Figure 1). The PSEUROT program[21,22] has been an important tool in the determination of the solution conformers of these furanose rings by analysis of the vicinal $^1H-^1H$ coupling constants of the ring hydrogen atoms. This program assumes a two-state approximation, where a North (N) and a South (S) conformer equilibrate via pseudorotation, rather than inversion through a high-energy eclipsed planar ring form. Each conformer can be described by its pseudorotational phase angle, P, and puckering amplitude, Φ_{max}. From a set of vicinal $^1H-^1H$ coupling constants obtained from a given five-membered ring, P can be calculated for both conformers along with the N/S population ratio. The identity and relative populations of the N and S conformers depend on several factors, including steric and stereoelectronic effects.[23,24] These factors also influence the distribution of rotamers about the C4−C5 bond of these ring systems. In the past, the hydroxymethyl group rotamer populations of several furanose-containing mono- and oligosaccharides have been calculated.[25−28] This was done by analysis of the coupling constants between the two pro-chiral C5 protons and the C4 proton, measured from the ^1H NMR spectra of these compounds. A generalized Karplus equation[29,30] was then used to determine the relative populations of the three rotamers. The three minimal staggered rotamers depicted in Figure 2 describe the C4−C5 bond conformation.

Although the majority of the D-arabinofuranose residues present in AG and LAM are in the α-configuration, β-D-arabinofuranosyl residues are also present. These moieties are typically found at the periphery of the polysaccharides, and their hydroxymethyl group is usually substituted with other groups that play key roles in the survival and pathogenicity of the organism.[11] For example, in the AG,

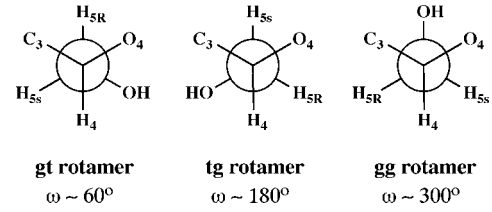

Figure 2. Definition of *gt*, *tg*, and *gg* rotamers about the C4−C5 bond. The quantity ω describes the dihedral angle between the endocyclic oxygen O4 and the hydroxyl group OH-5.

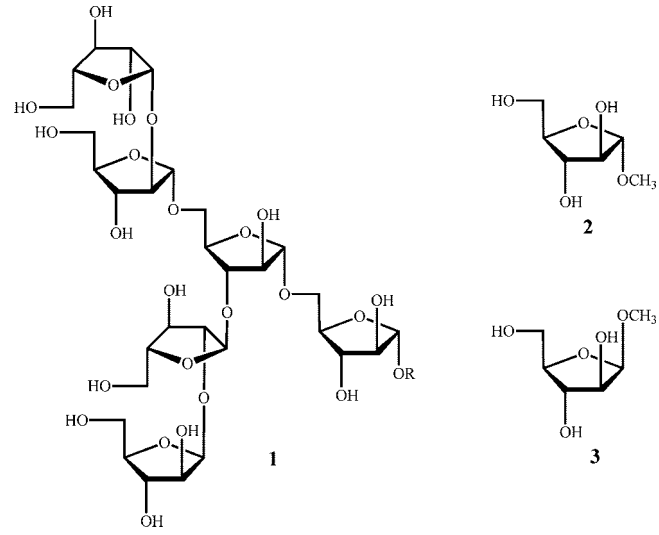

Figure 3. Hexasaccharide motif (**1**) found at the nonreducing termini of mycobacterial AG and LAM, methyl α-D-arabinofuranoside (**2**), and methyl β-D-arabinofuranoside (**3**).

this group is the site to which the mycolic acids are esterified,[11] while in the LAM a range of "capping" motifs are found attached to this position.[31]

Several structural investigations on mycobacterial arabinofuranosides have been carried out,[15−19] including various high-level *ab initio* and density functional theory (DFT) calculations. Our current interests lie in the study of larger oligomers of D-arabinofuranose, for which we have NMR data.[25,32] Of particular interest is a hexasaccharide motif found at the nonreducing end of AG and LAM (**1**, Figure 3), comprised of both α and β arabinofuranose residues. However, the size of these molecules renders their treatment with *ab initio* or DFT methods impractical. As a result, the use of force field models to probe the conformation of these oligosaccharides is the only practical way to model these systems. In previous conformational studies of methyl α-D-arabinofuranoside[33] (**2**, Figure 3) as well as similar investigations on pyranosides,[34−36] it was found that the use of the AMBER[37] force field in conjunction with the GLYCAM[38] parameter set was an effective method for modeling carbohydrates. Herein, we report our investigations on the use of this computational approach to study the conformation of methyl β-D-arabinofuranoside (**3**). In particular, we examine the ability of the method to reproduce the distribution of rotamers about the C4−C5 bond and the ring conformers as determined by NMR spectroscopy. In the course of these studies we demonstrated that the water model used had an

important influence on the ability of this method to reproduce experimentally determined conformer populations.

Methodology

The AMBER forcefield with the GLYCAM parameter set was employed for the description of methyl β-D-arabinofuranoside **3**. All molecular dynamics (MD) simulations were carried out using the *Sander* module in the AMBER 9.0 suite of programs,[37] and the electronic structure calculations were performed with Gaussian 03.[39]

Ring Averaged Charge Calculations. To carry out the MD simulations on **3**, partial atomic charges were required. Due to the flexibility of furanose rings, a novel ring-averaged approach developed by us,[33] which incorporates the effects of ring flexibility, was implemented to obtain partial charges for **3**. This method is a modification of the usual GLYCAM approach developed by Woods and workers.[36] The input geometry of **3** was obtained from crystallographic data,[40] and an *ab initio* geometry optimization was performed at the HF/6−31G* level of theory. An initial set of restrained partial atomic charges was obtained using the RESP approach.[41] After a 50 ns MD simulation, 200 random conformations were selected from the resulting trajectory, and a constrained *ab initio* geometry optimization (HF/6−31G*) was performed for each conformation, restricting the dihedral angles involving the hydroxyl protons to the values obtained from the simulations. For the 200 new conformations, each with unique ring geometry and torsion angles, a single point HF/6−31G* calculation was performed to obtain the RESP fit, and the final charge of each atom was calculated as an average. The value of the RESP restraint weight was set to 0.01, and fitting was only performed to the nonaliphatic hydrogen atoms.[42] The charges obtained from this procedure were ensemble averaged over several exocyclic torsions and ring conformations. The charges used in the simulations are provided in the Supporting Information.

Coupling Constant Analysis. An NMR spectrum of methyl β-D-arabinofuranoside **3** in D_2O solution was obtained using a Varian Inova 400 MHz spectrometer. Rotamer populations were calculated using a generalized Karplus relationship[30] represented by eq 1

$$^3J_{HH} = 14.63\cos^2\varphi - 0.78\cos\varphi + 0.60 + \sum_i \lambda_i\{0.34 - 2.31\cos^2[\xi_i\varphi + 18.4|\lambda_i|]\} \quad (1)$$

where λ_i is the difference in electronegativities of nonhydrogen substituents along the coupling path, and ξ_i is +1 or −1 depending on the relative orientation of substituents. The angle ϕ is the dihedral angle between the two coupled protons. A number of different calculations were carried out. In one, the angles used the values for ideally staggered rotamers (60°, 180°, and −60°). In another set of calculations, this angle was equal to a value corresponding to the most probable dihedral angle obtained from the respective MD simulations (e.g., 61°, 174°, and −61° for the TIP3P H_4-H_{5R} dihedral). This data are provided in the Supporting Information. Equation 1 produces values for limiting coupling constants of the individual rotamers. Due to rapid interconversion of rotamers, the experimentally observed vicinal couplings are the weighted sums of these values. This is represented by eqs 2−4, where X_i represents the mole fractions of each rotamer, and the coefficients are the limiting coupling constants calculated based on idealized staggered geometry:

$$^3J_{H_4-H_{5R}} = 0.9X_{gg} + 11.1X_{gt} + 4.5X_{tg} \quad (2)$$

$$^3J_{H_4-H_{5R}} = 2.7X_{gg} + 2.7X_{gt} + 11.1X_{tg} \quad (3)$$

$$1 = X_{gg} + X_{gt} + X_{tg} \quad (4)$$

Once a set of experimental couplings is obtained, eqs 2−4 can be simultaneously solved to produce the desired rotameric distribution.

Solution Simulations. A 200 ns molecular dynamics simulation of **3** was performed in a box of 264 TIP3P[43] water molecules under NPT conditions. The total box size was 22.771 × 25.372 × 25.544 Å. The temperature of the system was set to 300 K and the pressure to 1 atm using a constant temperature thermostat with the weak coupling algorithm (*ntt* = 1) and a constant pressure barostat with isotropic position scaling (*ntp* = 1). A cutoff of 8 Å was used for nonbonded interactions. Scaling parameters (SCNB and SCEE) were set to 1.0 in accordance with the GLYCAM approach. All simulations were carried out under NPT conditions using the SHAKE[44] algorithm to constrain all hydrogen-containing bonds. Prior to production dynamics, minimization of the water molecules was performed, followed by minimization of the whole system, 100 ps of annealing and 150 ps of equilibration. Ewald summation was used to handle long-range electrostatics.

Hydrogen Bonding Analysis. Hydrogen bond analysis of the 200 ns trajectory was performed using the *ptraj* module in the AMBER suite. All oxygen atoms in **3** were assigned as potential hydrogen bond donors, and all hydroxyl hydrogen atoms were assigned as potential acceptors. The criteria used for a hydrogen bond was a cutoff distance of 3.5 Å between the two heavy atoms and an angle cutoff of 120.0°. All intramolecular interactions were also specified in the analysis using the INCLUDESELF keyword.

Gas-Phase Simulations. A simulation of **3** was performed in the gas phase to highlight the importance of the effects of explicit solvation. The same simulation parameters were employed as those for the solution simulations. However, periodic boundary conditions and Ewald summation were not used. A cutoff of 18.0 Å was utilized for the long-range interactions.

TIP4P and TIP5P Simulations. Simulations of **3** using the TIP4P[43] and TIP5P[45] water models were also performed. Using TIP4P, a water box of 711 molecules with dimensions of 30.086 × 32.853 × 32.457 Å was used. For TIP5P, a box of 568 molecules was used with dimensions of 29.803 × 33.253 × 34.560 Å. All other parameters were identical to the TIP3P simulations.

Results and Discussion

Atomic Charges. Our modification of the usual GLYCAM approach for charge derivation, which incorporates the effects

Table 1. Experimental Rotameric Distributions about the C4−C5 Bond in **3**

	ideal geometry	TIP3P	GAS	TIP4P	TIP5P
X_{gt} (%)	57	55	58	56	54
X_{tg} (%)	8	10	6	8	12
X_{gg} (%)	35	35	36	36	34

of the ring flexibility, was described previously.[33] The charges obtained from this procedure are presented in the Supporting Information. An average rmsd of the carbon atoms of the ring based on the 200 conformations used in the ring averaging was calculated, and a value of 0.17 with a fluctuation of 0.07 was obtained. This parameter provides a measure of the ring flexibility of the system. To quantify the magnitude of the rmsd in terms of puckering, a correlation study was carried out that indicates what change in ring puckering corresponds to a particular value of rmsd. A large number of conformations (namely 100000) were selected for this correlation study from the simulation based on our ring-averaged atomic charges (discussed below). This number of conformations was chosen to obtain a statistically meaningful estimate.

C4−C5 Rotamer Populations. Using eqs 2−4 for ideally staggered rotamers, a distribution of 57:8:35 *gt*:*tg*:*gg* was obtained from the NMR data (Table 1). Moreover, experimental distributions using the most probable dihedral angle values ($H_4-C_4-C_5-H_{5S}$ and $H_4-C_4-C_5-H_{5R}$, see the Supporting Information) obtained from the MD simulations were also calculated; these results are reported in Table 1.

In our previous studies of methyl α-D-arabinofuranoside (**2**),[33] the length of the MD simulations required to obtain convergence of C4−C5 rotamer populations was established to be 200 ns. A convergence study of the rotamer populations in **3** as a function of simulation time is presented in Figure 4. As was observed for **2**, a simulation time of 200 ns was optimal for the convergence of rotamer populations in **3** to reasonable uncertainties (see the Supporting Information). Figure 5 shows a time-dependence study of the C4−C5 torsion angle and its associated distribution. Integration of the peaks in the histogram results in a distribution of 40:12:48 for the *gt*:*tg*:*gg* rotamers. The *gg* rotamer is found to be the most populated, a result that contradicts the experimentally observed rotamer population distributions (Table 1).

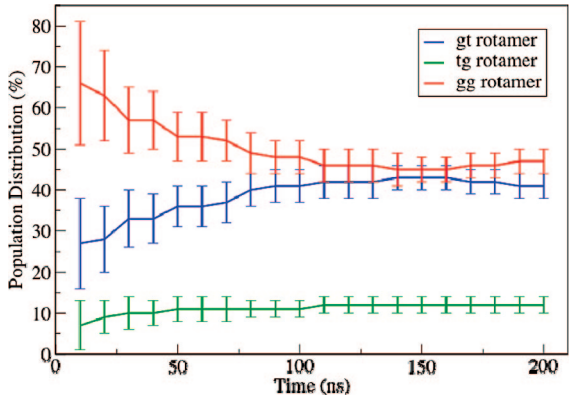

Figure 4. Convergence of the rotamer distribution of **1** as a function of simulation time in TIP3P water.

The discrepancy between the results from the MD simulation and experiment may be rationalized by solvation effects. In aqueous solution, it could be expected that the C5 hydroxyl group is heavily solvated by water molecules, rendering it too sterically demanding to be favorably oriented in the *gg* rotamer. In addition, solvation of this hydroxyl group would also diminish intramolecular hydrogen bonds present within the sugar that may stabilize the *gg* rotamer.

To assess intramolecular hydrogen bond patterns in the conformer ensemble of **3**, these interactions were analyzed as described in the Methodology section. The results of this analysis suggest that there exists intramolecular hydrogen bonding interactions within **3** that may be responsible for the discrepancy in the results between experiment and simulation. In the 200 ns trajectory, a hydrogen bond exists between O5 and H2 in 4.3% occupancy and between O2 and H5 in 1.1% occupancy (Figure 6, TIP3P). This occupancy of hydrogen bonds is most likely to occur in the *gg* rotamer where these particular hydrogen donors (H2 and H5) are in close proximity to the oxygen acceptors (O5 and O2, respectively). We hypothesize that this collective occupancy of 5.4% should be reduced or eliminated by competing *inter*molecular hydrogen bonds with water and therefore affect the difference in *gg* and *gt* populations. In other words, if the *gt* population is increased by 5.4% or more, and the *gg* population is decreased by the same amount, the populations will near experimental values. Other intramolecular H-bonds (e.g., O5···H3 and O4···H5) do exist but in minimal occupancy.

To probe further intramolecular hydrogen bonding in **3**, a gas-phase simulation was performed. Analysis of the resulting trajectory showed that there was, as expected, an overall increase in the intramolecular hydrogen bonding interactions compared to those observed in the TIP3P simulations (Figure 6, gas phase). Concomitantly, the rotamer distribution diverged further from the experimental data. The C4−C5 bond rotamer distributions from these gas-phase MD simulations are presented in Figure 7 and compared to results from TIP3P simulations and experiment. In the gas phase, the *gt* rotamer (23%) significantly decreased in population, while the *gg* (55%) and *tg* (22%) rotamer populations increased. This suggests a higher propensity for the *gg* and *tg* rotamers to form intramolecular hydrogen bonds compared with the *gt* rotamer. This deviation from experiment led to the implication that the TIP3P water model used in the simulations may be insufficient to provide an accurate representation of the aqueous solvation of **3**.

This result led to the examination of alternative water models for use in the simulations. A number of different potential functions for liquid water have been developed over the past several years.[46] Although many bear little resemblance to "real water", there exist models that are more sophisticated than TIP3P, which would generally give better agreement. TIP3P can be depicted as an effective rigid pair potential composed of Lennard-Jones (LJ) and columbic interaction terms, where the LJ site is on the oxygen atom and the charge sites are on the hydrogen atoms; it uses atom-centered point charges to represent the electrostatic interactions. As an alternative, TIP4P[43] is a branched and rigid water

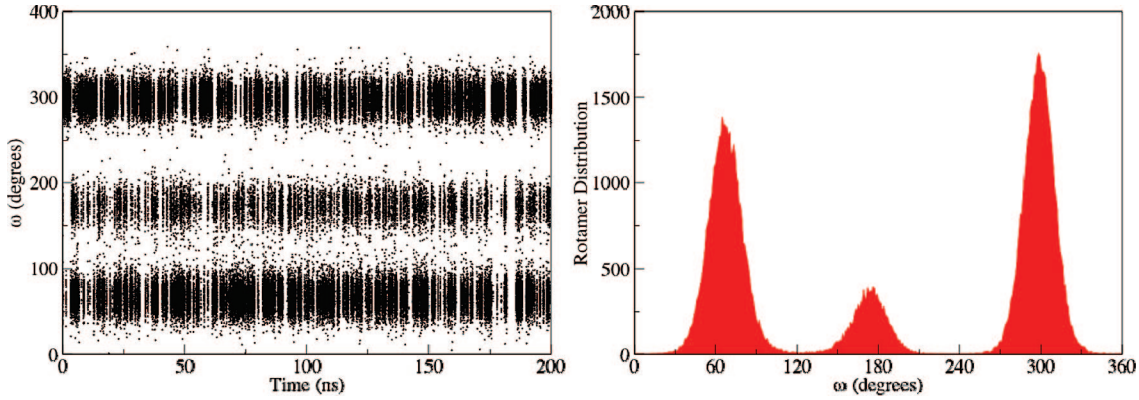

Figure 5. Time dependence of the C4−C5 torsion angle (left) and its associated distribution (right) in TIP3P water.

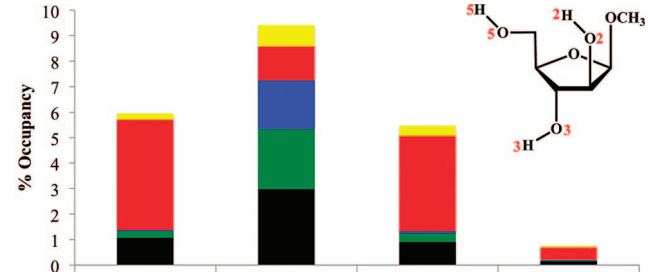

	TIP3P	Gas Phase	TIP4P	TIP5P
O5-H3	0.25	0.84	0.41	0.06
O5-H2	4.32	1.33	3.74	0.49
O3-H5	0.05	1.92	0.09	0.02
O4-H5	0.26	2.35	0.33	0.03
O2-H5	1.07	2.98	0.91	0.15

Figure 6. Percentage occupancy of intramolecular hydrogen bonds.

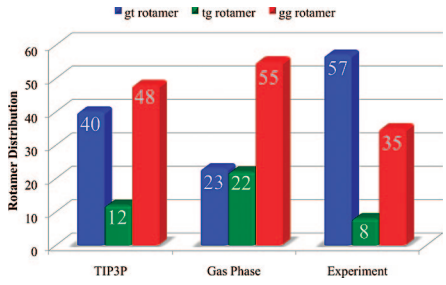

Figure 7. Rotamer population distribution of **1** in solution (TIP3P) and gas phase and their comparison to experiment.

model that has a LJ site on the oxygen and bare charge sites on the hydrogen atoms and along the bisector between the hydrogen atoms. Because this model utilizes more interaction sites, it provides an improved description of liquid water and thus may aid in obtaining a satisfactory computational outcome. Moreover, TIP5P[45] is a branched rigid model that utilizes an additional two charge sites that represent the electron lone pairs in "real" water. Although these models offer a better representation of water, their use in MD simulations would typically result in a significantly increased computational cost, as the number of interaction sites increases.

To study the effect of the water model on the conformational ensemble, MD simulations of **3** were performed using the TIP4P and TIP5P water models, at simulation times of 200 and 185 ns, respectively; the rotamer populations converged at these times (Figure 8). The distributions of the C4−C5 bond torsion angles of **3** in these two water models are presented in Figure 9; a comparison of the rotamer distributions obtained from all simulations is shown in Figure 10.

Gratifyingly, and in contrast to the results using TIP3P, the general trend in rotamer populations obtained from the TIP4P simulations parallels that found in experiment (*gt* > *gg* > *tg*); the calculated populations of the *gt* and *gg* rotamers are similar within the error bars. The *gt* rotamer is the most populated of the three, whereas the *tg* rotamer is the least populated. A similar trend was observed using the TIP5P water model. From these results we conclude that the use of the more refined water models in the simulations provides a conformational ensemble of C4−C5 bond rotamers in **3** that are in better agreement with experiment. Moreover, a comparison of the MD rotameric distributions with the experimental values obtained by using the most probable dihedral angle values from the respective simulations (Table 1) shows a slightly better agreement in each case when compared to the idealized geometry.

Hydrogen bond analysis of the resulting trajectories of the TIP4P and TIP5P simulations shows a decreased percentage in the occupancy of the intramolecular hydrogen bonds compared to that observed in the TIP3P simulations (Figure 6, TIP4P and TIP5P). With the TIP4P model, the O5···H2 hydrogen bond is 3.7% populated, whereas the O2···H5 hydrogen bond is 0.9% populated, levels that are reduced compared to the TIP3P simulations (4.3% and 1.1%, respectively). Although these differences are small, the better agreement with experiment demonstrates the superiority of the TIP4P water model for simulations of **3**. The formation of intramolecular hydrogen bonds is even more reduced in the TIP5P simulation − the overall percentage of these intramolecular interactions is extremely minor (a total of 0.75% occupancy) − suggesting that with this model intermolecular interactions with solvent molecules compete well with the formation of intramolecular hydrogen bonds. Therefore, this implies that the more sophisticated water models may provide a more accurate representation of the solvent effects involved in this system. Although this is not unexpected when comparing TIP4P and TIP5P to real water, the simulation results do demonstrate that the use of less

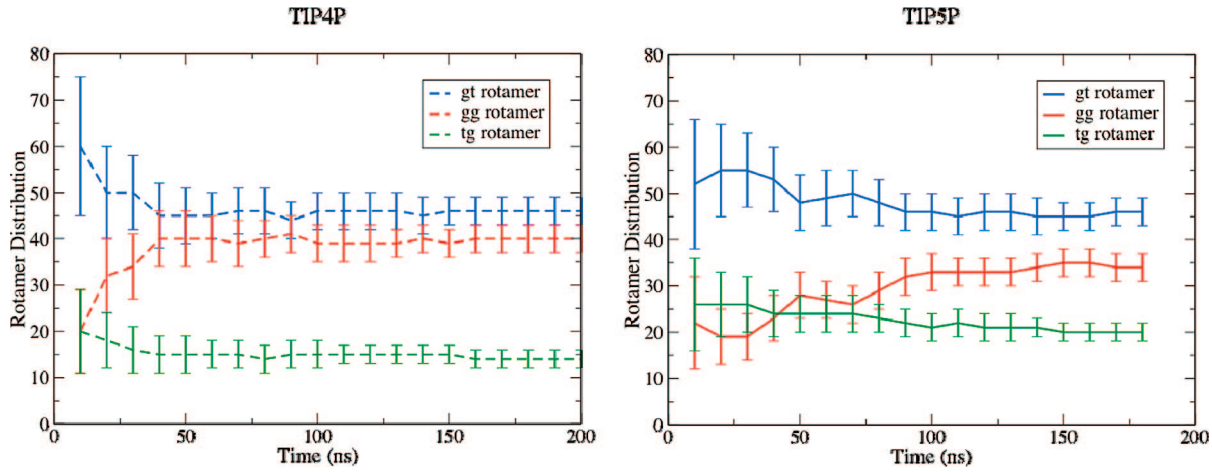

Figure 8. Convergence of the rotamer distribution of **1** as a function of simulation time in TIP4P (right) and TIP5P (left) water.

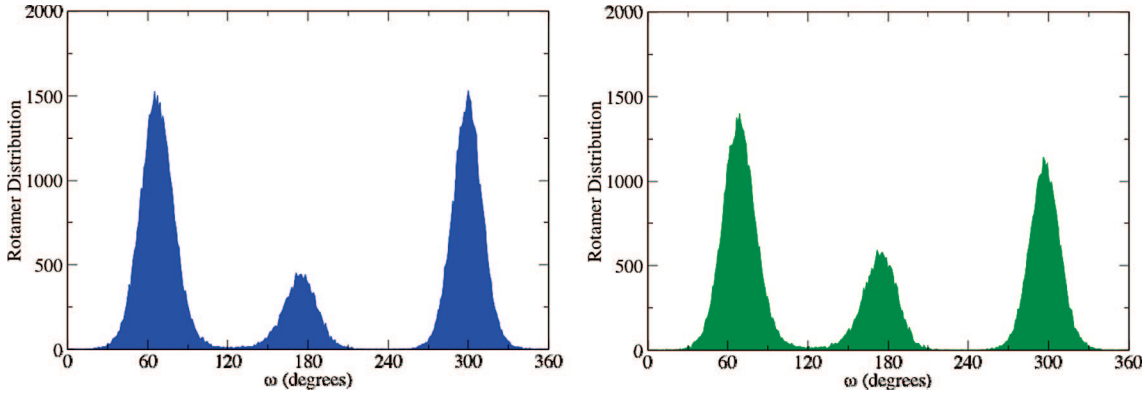

Figure 9. Distribution of the C4−C5 torsion angle in TIP4P (blue, left) and TIP5P (green, right) water.

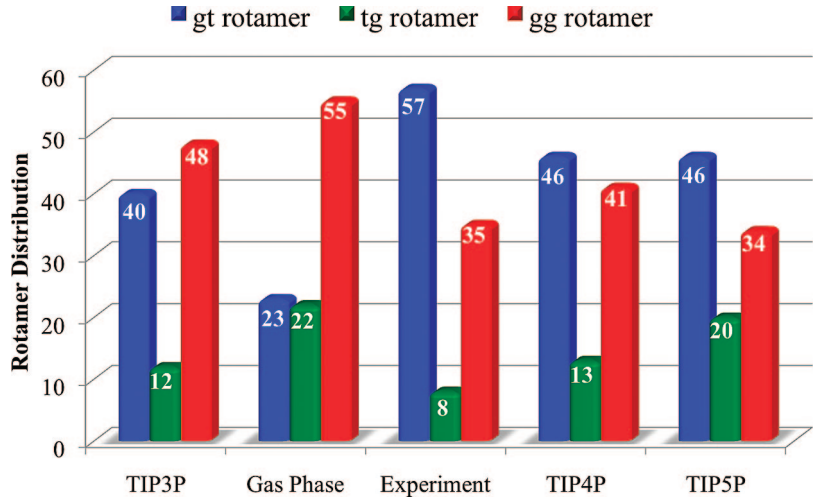

Figure 10. A summary of the distribution of rotamer populations about the C4−C5 bond of **3** in TIP3P water, gas phase, TIP4P water, and TIP5P water compared to experiment.

sophisticated water models is insufficient to represent the solvation of this particular system. Moreover, it was surprising to observe that this outcome is unique when compared to the α system **2**[33] where TIP3P was sufficient for good agreement with experiment.

Ring Conformer Populations. Having successfully identified simulation parameters that provided C4−C5 rotamer populations in good agreement with experiment, our attention turned to ring parameters in **3**, P and Φ_{max}. Figure 11 presents the variation in P, which describes the ring puckering, in all simulations; the inset shows the variation in puckering amplitude, Φ_{max}. The MD simulations correctly predict the two-state model generally used to model the solution conformation for furanoside ring systems. From the 200 ns trajectory, 55% of the conformations are present in the northern hemisphere of the pseudorotational itinerary (see

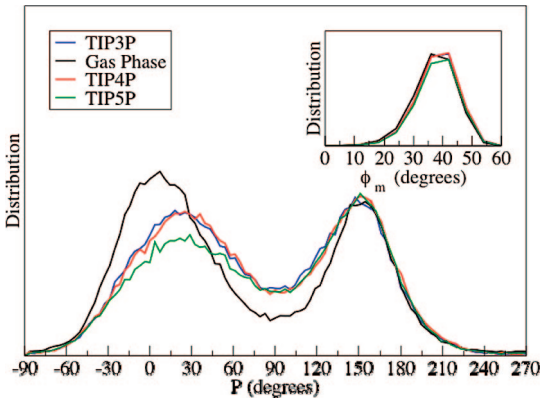

Figure 11. The distribution of the pseudorotational phase angle (*P*) for **3** in the gas phase, TIP3P water, TIP4P, and TIP5P water. The distribution of puckering amplitude, Φ_{max}, is given in the inset.

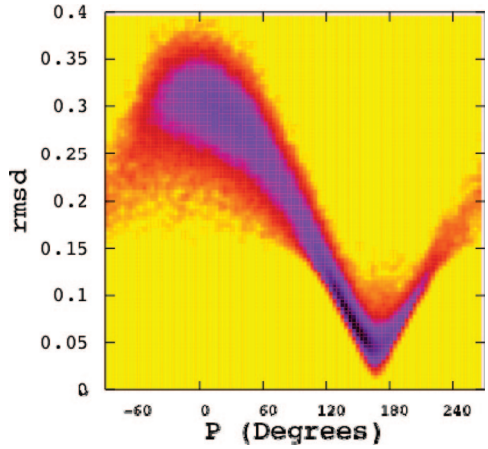

Figure 12. Joint probability distribution of the puckering angle (in degrees), *P*, and the rmsd (in Å) of the ring carbon atoms.

Figure 1), adopting pseudorotational phase angles of −90° to 60°. The remaining 45% of conformations exist in a range of *P* values from 120 to 240°. These magnitudes of the populations of these conformers do not correspond well with the experimental values ($P_N = -7°$, 86%; $P_S = 162°$, 14%) determined by PSEUROT.[12] However, the area of conformational space in the southern hemisphere is centered about $P = 160°$ and in the northern hemisphere about $P \approx 10°$, which corresponds well respectively to the S and N conformer determined for **3** experimentally. The distribution in Φ_{max} is centered about 39° in all simulations, and this corresponds well to earlier calculations on **3** as well as to the puckering parameters of this molecule in the crystal structure.[40]

The discrepancy in the pseudorotational phase angles could possibly arise from our modification of the standard GLYCAM approach to derive the partial atomic charges. Furanosides are flexible molecules, and thus, a single conformation cannot solely be used for the charge derivation. Rather, charges must be averaged over a number of rings to better represent all the conformations accessible to the system.[33] Figure 12 illustrates the correlation between the rmsd of the ring atoms and the distribution of the puckering angle, *P*. The graph indicates that an rmsd of 0.17 as obtained in the ring-averaged charge derivation procedure corresponds to a change of more than 100° in *P*. Fluctuations in the rmsd result in even greater changes in the ring puckering. This result is not unexpected, as previous simulations on **2** also yielded similar variations in *P*. Unlike our previous results, however, simulations on **3** suggested that the two-state conformational model for assessing ring conformation using PSEUROT *is* valid. Therefore, another possible source of discrepancy in *P* compared to experiment is that the generalized Karplus equation used in the PSEUROT analysis of **3** may not be accurate for this ring system. This could be circumvented by the calculation of Karplus curves specific for each coupling pathway in β-arabinofuranoside rings, using theoretical methods.[47,48] Moreover, access to accurate Karplus curves tailored to **3** would allow a direct comparison of ring $^3J_{H,H}$ obtained from NMR spectroscopy, with those obtained from the conformational ensemble generated by AMBER/GLYCAM MD simulations. Such an approach may circumvent possible sources of error entailed by the PSEUROT approach. It appears that Karplus relationships more specific to **3** are essential. An attempt to calculate $^3J_{H,H}$ of **3** from the conformer distribution provided by the MD simulations using the generalized Karplus equations[30] led to poor agreement with experiment (data not shown).

Conclusions

In this paper, the combined AMBER/GLYCAM forcefield model was applied to simulations of methyl β-D-arabinofuranoside (**3**). A recently developed method for the calculation of atomic charges was used to take into account the flexibility of the furanose ring in **3**. Initial simulations with TIP3P water model yielded C4−C5 rotamer populations that were not in good agreement with experimental data, and hydrogen bond analysis as well as gas-phase simulations suggested that more sophisticated water models were required for the proper representation of the solvation of **3**. The TIP4P and TIP5P water models were then employed, and both demonstrated good agreement of the C4−C5 rotamer distribution with the experimental results. Analysis of the ring puckering showed that although the magnitude of populations of the two low energy conformations are different than experiment, good agreement was obtained with respect to the identity of each conformer as well as the puckering amplitude (Φ_{max}). The discrepancy in puckering results may be attributed to the charge derivation procedure or an inaccurate Karplus relationship that was used in the analysis of experimental $^3J_{H,H}$ data. Having successfully applied the AMBER/GLYCAM approach to investigate the conformation of **3**, this method will be used in the conformational studies of larger furanose containing oligosaccharides, such as **1**. In addition, novel Karplus equations for each $^1H-^1H$ coupling fragment in **3** are currently being developed using theoretical methods.

Acknowledgment. This work was supported by the Alberta Ingenuity Centre for Carbohydrate Science and the Natural Sciences and Engineering Research Council of Canada.

Supporting Information Available: Calculated partial atomic charges, with standard deviations; MD simulations convergence criteria, with errors in rotamer populations; coupling constants for **3**, compared to previously reported values; values for the most probable dihedral angles in each simulation; and comparison of MD rotamers and experimental rotamers in each case. This material is available free of charge via the Internet at http://pubs.acs.org.

References

(1) Bloom, B. B.; Murray, C. L. J. *Science* **1992**, *257*, 1055–1064.

(2) Zhang, Y. *Annu. Rev. Pharmacol. Toxicol.* **2005**, *45*, 529–564.

(3) Hamasur, B.; Källenius, G.; Svenson, S. B. *Vaccine* **1999**, *17*, 2853–2861.

(4) Dietrich, J.; Lundberg, C. V.; Andersen, P. *Tuberculosis* **2006**, *86*, 163–168.

(5) Williams, D. H. *Nat. Prod. Rep.* **1996**, *13*, 469–477.

(6) Gadebusch, H. H.; Stapley, E. O.; Zimmerman, S. B. *Crit. Rev. Biotechnol.* **1992**, *12*, 225–243.

(7) Woodin, K. A.; Morrison, S. H. *Pediatr. Rev.* **1994**, *15*, 440–447.

(8) Janin, Y. L. *Bioorg. Med. Chem.* **2007**, *15*, 2479–2513.

(9) Lowary, T. L. *Mini Rev. Med. Chem.* **2003**, *3*, 689–702.

(10) Barry, C. E. *Biochem. Pharmacol.* **1997**, *54*, 1165–1172.

(11) Brennan, P. J.; Nikaido, H. *Annu. Rev. Biochem.* **1995**, *64*, 29–63.

(12) Houseknecht, J. B.; Lowary, T. L.; Hadad, C. M. *J. Phys. Chem. A* **2003**, *107*, 5763–5777.

(13) Connell, N. D.; Nikaido, H. In *Tuberculosis: Pathogenesis, Protection and Control*; Bloom, B. R., Ed.; American Society for Microbiology: Washington, DC, 1994; pp 333−352.

(14) Draper, P., Daffé, M. The Cell Envelope of *Mycobacterium tuberculosis* with special reference to the capsule and outer permeability barrier. In *Tuberculosis and the Tubercle Bacillus*; Cole, S. T., Eisenach, K. D., McMurray, D. N., Jacobs, W. R., Jr., Eds.; American Society for Microbiology: Washington, DC, 2005; pp 261−273.

(15) Gordon, M. T.; Lowary, T. L.; Hadad, C. M. *J. Am. Chem. Soc.* **1999**, *121*, 9682–9692.

(16) McCarren, P. R.; Gordon, M. T.; Lowary, T. L.; Hadad, C. M. *J. Phys. Chem. A* **2001**, *105*, 5911–5922.

(17) Gordon, M. T.; Lowary, T. L.; Hadad, C. M. *J. Org. Chem.* **2000**, *65*, 4954–4963.

(18) Houseknecht, J. B.; Lowary, T. L.; Hadad, C. M. *J. Phys. Chem. A* **2003**, *107*, 372–378.

(19) Houseknecht, J. B.; McCarren, P. R.; Lowary, T. L.; Hadad, C. M. *J. Am. Chem. Soc.* **2001**, *123*, 8811–8824.

(20) Altona, C.; Sundaralingam, M. *J. Am. Chem. Soc.* **1972**, *94*, 8205–8212.

(21) *PSEUROT*, *version 6.2*; Gorlaeus Laboratories, University of Leiden: Leiden, NL, 1995.

(22) Deleeuw, F.; Altona, C. *J. Comput. Chem.* **1983**, *4*, 428–437.

(23) Plavec, J.; Tong, W.; Chattopadhyaya, J. *J. Am. Chem. Soc.* **1993**, *115*, 9734–9746.

(24) Plavec, J.; Thibaudeau, C.; Chattopadhaya, J. *Pure Appl. Chem.* **1996**, *11*, 2137–2144.

(25) D'Souza, F. W.; Ayers, J. D.; McCarren, P. R.; Lowary, T. L. *J. Am. Chem. Soc.* **2000**, *122*, 1251–1260.

(26) Callam, C. S.; Lowary, T. L. *J. Org. Chem.* **2001**, *66*, 8961–8972.

(27) Joe, M.; Sun, D.; Taha, H.; Completo, G. C.; Croudace, J. E.; Lammas, D. A.; Besra, G. S.; Lowary, T. L. *J. Am. Chem. Soc.* **2006**, *128*, 5059–5072.

(28) Wu, G. D.; Serianni, A. S.; Barker, R. *J. Org. Chem.* **1983**, *48*, 1750–1757.

(29) Altona, C.; Ippel, J. H.; Hoekzema, A. J. A. W.; Erkelens, C.; Groesbeek, M.; Donders, L. A. *Magn. Reson. Chem.* **1989**, *27*, 564–576.

(30) Altona, C.; Francke, R.; de Haan, R.; Ippel, J. H.; Daalmans, G. J.; Hoekzema, J. A. W.; van Wijk, J. *Magn. Reson. Chem.* **1994**, *32*, 670–678.

(31) Nigou, M.; Gilleron, M.; Puzo, G. *Biochimie* **2003**, *85*, 153–166.

(32) Rademacher, C.; Shoemaker, G. K.; Kim, H. S.; Zheng, R. B.; Taha, H.; Liu, C.; Nacario, R. C.; Schriemer, D. C.; Klassen, J. S.; Peters, T.; Lowary, T. L. *J. Am. Chem. Soc.* **2007**, *129*, 10489–10502.

(33) Seo, M.; Castillo, N.; Ganzynkowicz, R.; Daniels, C. R.; Woods, R. J.; Lowary, T. L.; Roy, P.-N. *J. Chem. Theory Comput.* **2008**, *4*, 184–191, and appropriate references within.

(34) Kirschner, K. N.; Woods, R. J. *Proc. Natl. Acad. Sci. U.S.A.* **2001**, *98*, 10541–10545.

(35) Gonzalez-Outeiriño, J.; Kirschner, K. N.; Thobhani, S.; Woods, R. J. *Can. J. Chem.* **2006**, *84*, 569–579.

(36) Basma, M.; Sundara, S.; Calgan, D.; Vernali, T.; Woods, R. J. *J. Comput. Chem.* **2001**, *22*, 1125–1137.

(37) Case, D. A.; Cheatham, T. E.; Darden, T.; Gohlke, H.; Luo, R.; Merz, K. M.; Onufriev, A.; Simmerling, C.; Wang, B.; Woods, R. J. *J. Comput. Chem.* **2005**, *26*, 1668–1688.

(38) Woods, R. J.; Dwek, R. A.; Edge, C. J.; Fraserreid, B. *J. Phys. Chem.* **1995**, *99*, 3832–3846.

(39) *Gaussian 03*, *Revision C.02*; Frisch, M. J.; Trucks, G. W.; Schlegel, H. B.; Scuseria, G. E.; Robb, M. A.; Cheeseman, J. R.; Montgomery, J. A., Jr.; Vreven, T.; Kudin, K. N.; Burant, J. C.; Millam, J. M.; Iyengar, S. S.; Tomasi, J.; Barone, V.; Mennucci, B.; Cossi, M.; Scalmani, G.; Rega, N.; Petersson, G. A.; Nakatsuji, H.; Hada, M.; Ehara, M.; Toyota, K.; Fukuda, R.; Hasegawa, J.; Ishida, M.; Nakajima, T.; Honda, Y.; Kitao, O.; Nakai, H.; Klene, M.; Li, X.; Knox, J. E.; Hratchian, H. P.; Cross, J. B.; Bakken, V.; Adamo, C.; Jaramillo, J.; Gomperts, R.; Stratmann, R. E.; Yazyev, O.; Austin, A. J.; Cammi, R.; Pomelli, C.; Ochterski, J. W.; Ayala, P. Y.; Morokuma, K.; Voth, G. A.; Salvador, P.; Dannenberg, J. J.; Zakrzewski, V. G.; Dapprich, S.; Daniels, A. D.; Strain, M. C.; Farkas, O.; Malick, D. K.; Rabuck, A. D.; Raghavachari, K.; Foresman, J. B.; Ortiz, J. V.; Cui, Q.; Baboul, A. G.; Clifford, S.; Cioslowski, J.; Stefanov, B. B.; Liu, G.; Liashenko, A.; Piskorz, P.; Komaromi, I.; Martin, R. L.; Fox, D. J.; Keith, T.; Al-Laham, M. A.; Peng, C. Y.; Nanayakkara, A.; Challacombe, M.; Gill, P. M. W.; Johnson, B.; Chen, W.; Wong, M. W.; Gonzalez, C.; Pople, J. A. Gaussian, Inc.: Wallingford, CT, 2004.

(40) Evdokimov, A.; Gilboa, A. J.; Koetzle, T. F.; Klooster, W. T.; Schultz, A. J.; Mason, S. A.; Albinati, A.; Frolow, F. *Acta Crystallogr., Sect. B: Struct. Sci.* **2001**, *57*, 213–220.

(41) Bayly, C. I.; Cieplak, P.; Cornell, W. D.; Kollman, P. A. *J. Phys. Chem.* **1993**, *97*, 10269–10280.

(42) Woods, R. J.; Chappelle, R. *J. Mol. Struct.* **2000**, *527*, 149–156.

(43) Jorgensen, W. L.; Chandrasekhar, J.; Madura, J. D.; Impey, R. W.; Klein, M. L. *J. Chem. Phys.* **1983**, *79*, 926–935.

(44) Ryckaert, J. P.; Ciccotti, G.; Berendsen, H. J. C. *J. Comput. Phys.* **1977**, *23*, 327–341.

(45) Mahoney, M. W.; Jorgensen, W. L. *J. Chem. Phys.* **2000**, *112*, 8910–8922.

(46) Wallqvist, A.; Mountain, R. D. *Rev. Comput. Chem.* **1999**, *13*, 183–247.

(47) Stenutz, R.; Carmichael, I.; Widmalm, G.; Serianni, A. S. *J. Org. Chem.* **2002**, *67*, 949–958.

(48) Zhao, H.; Pan, Q.; Zhang, W.; Carmichael, I.; Serianni, A. S. *J. Org. Chem.* **2007**, *72*, 7071–7082.

CT800384H